NASA Technical Memorandum 79074

ANALYSIS OF RADIATION PATTERNS OF INTERACTION TONES GENERATED BY INLET RODS IN THE JT15D ENGINE

M. F. Heidmann, A. V. Saule,
and J. G. McArdle
Lewis Research Center
Cleveland, Ohio

TECHNICAL PAPER to be presented at the
Fifth Aeroacoustics Conference
sponsored by the American Institute of Aeronautics
and Astronautics
Seattle, Washington, March 12-14, 1979

ANALYSIS OF RADIATION PATTERNS OF INTERACTION TONES GENERATED BY INLET RODS IN THE JT15D ENGINE

M. F. Heidmann, A. V. Saule, and J. G. McArdle
National Aeronautics and Space Administration
Lewis Research Center
Cleveland, Ohio

E-9891

Abstract

Interaction tones were intentionally generated by circumferential arrays of equally spaced rods that protrude radially from the inlet wall near the face of the 28-blade fan. Arrays of 28 and 41 rods, selected to give specific far field radiation properties, were tested. The expected properties were readily apparent in the measured radiation patterns. A more detailed analysis of the test data showed both the precision and limitations of the applied acoustic theory. Rods protruding 23 percent of the radius predominantly generated only lowest radial order modes, as expected. Measured and predicted radiation patterns were generally in good agreement. The agreement, however, depended on a significant degree of implied refraction due to inlet velocity gradients. Refraction, if present, would impact static-flight noise comparisons.

Symbols

$A_{m,\mu}$	amplitude coefficient for (m,μ) mode in directivity function (eq. 3), N/m^2
B	number of rotor blades
C_0	velocity of sound, m/sec
C_m	apparent velocity of a mode, m/sec
f_1	directivity transformation function (eq. 6)
$J_m(\ ),$ $J'_m(\ )$	Bessel function and its derivative of first kind and order m for argument ( ),
K	integer
k	frequency parameter, equal to BM_T for BPF tone
$k'_{m,\mu}$	mode eigenvalue, $J'_m(k'_{m,\mu}) = 0$
m	circumferential order of a mode
M	mass flow Mach number (positive in engine flow direction)
M_T	tangential tip Mach number of rotor blade
$p_{m,\mu}$	far-field acoustic pressure of (m,μ) mode, N/m^2
V	number of stationary vanes or rods
μ	radial order of a mode
ζ	cutoff ratio
ϕ_i, ϕ_r	incident and refracted angles at an interface, deg
$\phi_1,$ $\phi_2,$ ϕ_3	far-field directivity angles of the acoustic mode radiated pressure assuming no mass flow, mass flow everywhere and duct mass flow alone, respectively
$(\phi_1)_p,$ $(\phi_2)_p,$ $(\phi_3)_p$	directivity angles ϕ_1, ϕ_2 and ϕ_3 at the approximate peak level of $p_{m,\mu}$

Introduction

The radiation patterns of blade passage frequency (BPF) tones generated by two configurations of rods placed near the fan in an engine inlet are analyzed in this paper. The study was conducted with a JT15D engine that is being tested at NASA LeRC as part of a comprehensive program with other organizations. An objective of the overall program is to resolve the discrepancies between the far-field acoustic signatures obtained during flight and during ground static tests. Tests of the engine at LeRC are being conducted with various inflow control devices (ICD's) to simulate the clean inflow and acoustic signatures of the engine in flight. The ICD's consist of screen and honeycomb structures that must transmit both acoustic radiation and the engine flow. As a part of that study a dominant additional BPF tone generated within an operating engine was required to evaluate the acoustic transmission properties of the ICD's. The additional tone was generated by the inlet rods. Results of the transmission study are reported in Ref. 1. The generation of an additional tone with inlet rods, however, also provided an opportunity to experimentally verify some theoretical predictions of interaction tone generation and propagation. The purpose of this paper is to compare measured and predicted propagation and radiation properties of interaction tones generated by the rods.

In this paper the experimental aspects of the engine study relevant to the data analysis are initially summarized. Analyses and results are then presented from essentially two perspectives. One is qualitative and the other more explicit. In the qualitative approach the concepts and objectives used to select rod configurations suitable for ICD evaluation are discussed and some measured far-field radiation patterns are shown that confirm the expected results. In the other, the experimental study is discussed with the context of more explicit acoustic theory and detailed analyses of the measured radiation patterns are presented.

Experimental Study

The test data analysed in this paper were acquired in a study reported in Ref. 1 where two ICD's were evaluated in static tests of a JT15D engine. What follows is a summary, pertinent to the present analysis, of the experimental aspects of that study.

The inlet configuration of the JT15D engine used in the study is schematically shown in Fig. 1. Acoustic data to be used were obtained without rods as shown in Fig. 1 and with circumferential arrays of equally spaced rods protruding from the inlet wall near the fan face as schematically shown in Fig. 2. Data from both the 28 and 41 rod arrays will be used. Some test data with a short inlet length, obtained by removing the 4 inch cylindrical section shown in Fig. 1, will also be examined.

As will be detailed later the JT15D engine as tested is designated as having tone cutoff for the fan in the bypass section. More specifically, for the rotor blade and the bypass stator vane numbers

listed in Fig. 1 the BPF interaction tone should not propagate at subsonic tip speeds. The BPF interaction tone for the core section, however, is not cutoff. When tone cutoff is predicted to occur the phenomenon is generally obscured in static engine tests by a tone caused by rotor interactions with inflow distortions. Two ICD's were tested with the JT15D engine at NASA LeRC[1] to eliminate this distortion noise source. An external ICD, designated ICD No. 1, proved to be most effective for this purpose. Figure 3 shows ICD No. 1 installed on the engine. As reported in Ref. 1, this ICD substantially reduced the inflow distortion tone level and had good noise transmission properties. It caused little or no change in far-field noise level or directivity of the tone noise produced by the rods. The data obtained with ICD No. 1, therefore, will be exclusively analyzed in this study because the tone noise generated by the rods is more clearly observable using this data.

The engine tests were conducted at the NASA LeRC Vertical Lift Fan Facility which is equipped to evaluate both acoustic and aerodynamic performance. Some of the engine performance variables pertinent to the acoustic analysis are shown as a function of engine speed in Fig. 4. An exhaust muffler, evident in Fig. 3, was used to eliminate off engine noise from the far-field data. Ground level microphones located on a 90 foot radius throughout the forward quadrant provided the basic acoustic results although supplemental pole mounted microphones were used occasionally. Acoustic and aerodynamic performance data were recorded on tape and processed using the system developed for the facility. Acoustic data to be used primarily consist of 1/3 octave band levels of the BPF tone adjusted to free-field and a 30.5 m (100 ft) radius and with atmospheric attenuation removed. Tests were made at several engine speeds for each configuration and generally repeated at least twice. Averaged acoustic data will be used when possible.

Qualitative Objectives and Results

The concepts and objectives used to select the arrays of rods to evaluate the ICD's are discussed in this section and some test data showing the soundness of the approach are presented. In the discussion a qualitative knowledge of some aspects of the acoustic theory to be presented later is assumed.

Rod Selection

Selection of the number of rods used in the arrays was based on a preliminary acoustic analysis where possible propagating modes and their far field directivity patterns were qualitatively predicted. Two separate arrays of rods were selected in this process. One array consisted of 28 rods. This array was predicted to give plane wave and axisymmetric modes that are highly propagating and thus was expected to give a high tone level. The bulk of the acoustic energy from such modes was expected to beam along the engine inlet axis. If, however, the tone level from the 28 rods were sufficiently high it could exceed that of other engine noise throughout the inlet quadrant of the engine. If not, tone dominance and evaluation of ICD acoustic transmission would be limited to a region near the inlet axis.

In contrast to the nonspinning modes generated by 28 rods, a tone with spinning modes, as often experienced in engine noise, was also desired for ICD evaluations. A 41 rod array was selected for this purpose. The selection criteria involved not only spinning modes but also a radiation pattern that would clearly show directivity changes caused by an ICD. Such directivity changes are best detected by the angular displacement of a distinctive feature (abrupt change in level with angle) in a directivity pattern. Ideally, the angular position of the distinctive feature within the directivity pattern should be controllable to fully evaluate ICD transmission properties. Tone energy contained in a single spinning mode that is near cutoff at a low engine speed and more highly propagating as speed is increased satisfies the above criteria. For such a mode the radiation beams toward the sideline at low engine speed and progressively beams closer to the inlet axis as speed increases.

The 41 rod array generates such a mode. An analysis showed that no other number of rods less than 41 will give the desired radiation properties. In reality, higher radial order modes of the expected mode may also be generated at high engine speeds. If this occurs, the beamed radiation will broaden in the direction toward the sideline, however, a distinctive frontal edge in the radiation pattern should always be evident.

Qualitative Discussion of Results

Figure 5 shows tone radiation patterns measured using ICD No. 1 both with and without the arrays of rods.[1] The shaded area in the figure is the difference between the levels with and without the rods and is indicative of the tone noise generated by the rods. The 28 rod array (Fig. 5(a)), caused the largest increase in tone level in the region near the engine inlet axis at all engine speeds and qualitatively confirms the prediction of plane wave and highly propagating axisymmetric modes. The tone is also seen to be dominant near the sideline, however, this dominance did not occur in tests without an ICD.

The results for the 41 rod array are shown in Fig. 5(b). The beamed radiation is seen to progressively advance toward the inlet axis with an increase in engine speed. The data qualitatively confirm the prediction of a single mode near cutoff at low speeds propagating toward the sideline and its progressive shift toward the inlet axis with increasing engine speed. Results with both the 28 and 41 rod arrays show that the qualitative criteria specified for the ICD acoustic transmission study were satisfied.

This study using inlet rods is one of few demonstrations wherein distinctive radiation patterns were obtained for a few known modes propagating from a relatively high flow Mach number inlet. Although qualitative agreement between theory and experiment was evident, the data warrant a more detailed acoustic analysis with regard to current theories of modal generation, propagation and radiation. Discrepancies, if significant, could impact the predictions of aircraft flight noise. A more detailed analysis of the results follows.

Propagation and Radiation Concepts

This section of the report describes the engine study within the context of more explicit acoustic theory and provides the theoretical background for the subsequent analysis and discussion of the test data.

Interaction Mode Generation

The tone noise generated when either rotor wakes interact with stator vanes or when stator or rod wakes interact with a rotor can be described in terms of acoustic modes. As presented in Ref. 2, a specific mode is identified by its circumferential, m, and radial, μ, order and commonly designated the (m,μ) mode. The m order of the mode for the BPF tone generated when V rods interact with B rotor blades is given by

$$m = B - KV \qquad (1)$$

where K is any integer.

A basic discriminator regarding mode propagation is the cutoff ratio ξ given by

$$\xi = \frac{BM_T}{k'_{m,\mu}} \Big/ \sqrt{1 - M^2} \qquad (2)$$

where M_T and M are the rotor tip and duct flow Mach numbers, respectively, and $k'_{m,\mu}$ is the mode eigenvalue. Propagation is only possible when ξ is greater than unity.

Basic Engine Configuration. Figure 6 shows the propagating interaction modes for the BPF tone of the JT15D engine without inlet rods. No propagating modes are generated by the interaction of the rotor with the bypass stators (B = 28, V = 66) within the engine operating speed range (the BPF tone is cutoff). The interaction of the rotor with the core stator blades (B = 28, V = 33) however, can generate m = 5 modes of increasing radial order as fan speed is increased as shown in Fig. 6. The rotor alone (B = 28, V = 0) can also generate a propagating mode above a fan speed of about 12,600 rpm (Fig. 6). Although these modes for the BPF tone may occur with the basic engine configuration they should remain fixed and not influence data comparisons with and without inlet rods.

28 Rod Array. Figure 7 shows the propagating modes for the interaction of 28 inlet rods with the rotor (B = 28, V = 28). Only axisymmetric (m = 0) modes are possible due to this interaction. The (0,0) mode is commonly designated the plane wave mode because its pressure amplitude is uniform over the duct cross section. This plane wave mode is possible at all fan speeds ($\xi = \infty$) with 28 rods. The cutoff condition for the higher radial orders of the m = 0 modes vary with fan speed as shown in Fig. 7.

41 Rod Array. Figure 8 shows the propagating modes for the interaction of 41 rods with the rotor (B = 28, V = 41). Only the m = 13 modes are possible due to this interaction. The lowest radial order mode (13,0) exceeds a cutoff ratio of unity at a fan speed near engine idle conditions. Higher radial order modes are possible at higher fan speeds.

The design intent for the 41 rods was to generate a single spinning mode at or near engine idle conditions and to minimize the number of modes at higher speed. The intent was satisfied as shown in Fig. 8. The intent cannot be satisfied by any number of rods less than 41.

Modal Power. The preceding analysis of cutoff properties primarily indicates whether modes can propagate. The acoustic power content of the propagating mode depends on details of the interaction process. Such an analysis has been performed[3] although the results have not as yet been coordinated with this study. The general approach in such analyses, however, is to match the radial profile of the forcing or excitation process with weighted combinations of the possible modes each with its unique radial variation in acoustic properties within a duct. Qualitatively, modal generation is thought to be most efficient when the radial profile of the acoustic source strength and that of the pressure amplitude characterizing a mode are identical.

Radial profiles of sound pressure level inside a circular duct for families of m = 0 and m = 13 modes are shown in Fig. 9(a). Except for the plane wave mode (0,0) with its uniform level, the modes are characterized by radial lobes. Each of these lobes are labelled positive or negative to indicate relative regions of reinforcement and rarefaction similar to that in organ pipe resonance. The modes as labelled are in-phase relative to each other according to normal analytical convention. A successive in-phase summation of radial order modes as labelled in Fig. 9(a) would alternately increase and decrease the pressure at the wall.

For the m = 13 order modes the concentration of acoustic energy is seen to progress from the wall toward the axis with increasing radial order. The interaction process from rods protruding 2.7 inches from the wall (28 percent of the radius) would appear to preferentially excite only the lowest or lower radial orders of the m = 13 modes.

For the m = 0 order modes, similar arguments are not obvious because acoustic power is substantial at the axis for all modes. Acoustic energy can be concentrated at the wall, however, by a summation of modes. Figure 9(b), for example, shows a summation of the (0,0) mode and the (0,1) mode phase shifted 180°. The summation suppresses the acoustic energy at the axis. A summation of additional modes, properly phased, would increase the concentration of acoustic energy at the wall. It is probable, therefore, that 2.7 inch rods will at least excite the (0,0) and either the (0,1) or another low radial order mode phase related by 180°.

Amplitude profiles for m = 5 and m = 28 modes of the BPF tone expected from the engine core and from the rotor alone, respectively, are similar to those for m = 13 shown in Fig. 9. They suggest that the core tone sources will preferentially excite higher radial order modes since the excitation is located near the hub. Tones generated by rotor interactions with inflow distortions (presumed to be probable at all radii) appear to exhibit no modal preference.[4]

Far-Field Radiation

An objective of this paper is to compare measured and predicted far-field radiation patterns. There is, however, no reported method that gives precise radiation patterns of a mode propagating from a bellmouth inlet on an operating engine under static test conditions. Some approximations must be used. The predictions to be used in this study are based on the techniques employed by Candel,[5] Homicz and Lordi[6] and expanded upon by Rice, et al.[7] The prediction procedure used and to be described consists of the following steps: (1) Calculate radiation patterns assuming no mass flow anywhere; (2) Adjust the patterns for the case of flow everywhere (duct and environment) by a transformation of variables; (3) Adjust the patterns for the case of internal duct flow alone by removing the external environmental convective effect; and (4) Examine mass flow processes near the inlet face for possible refractive effects on directivity. Angular adjustments alone are used in steps (2) and (3). Level changes will be neglected.

No Flow. The closed form analytical solutions for the radiation from a flanged duct without flow will be used for convenience. Wiener-Hopf solutions for a flangeless duct may be more appropriate for the engine inlet, however, the complexity of obtaining such solutions is not warranted at this time. Patterns predicted with and without a flange differ negligibly except in the region normal to the duct axis.[8]

A directivity expression for the far-field acoustic pressure, $p_{m,\mu}$, as a function of inlet angle ϕ, as used in Ref. 9, is given by

$$p_{m,\mu} = A_{m,\mu} \frac{J_m(k'_{m,\mu})(\bar{k} \sin \phi_1) J'_m(\bar{k} \sin \phi_1)}{(k'_{m,\mu})^2 - (\bar{k} \sin \phi_1)^2} \qquad (3)$$

The properties of this function are displayed in Fig. 10 for families of $m = 0$ and $m = 13$ modes. Acoustic sound pressure level is shown as a function of $\bar{k} \sin \phi_1$, with $A_{m,\mu}$ assumed constant for each family of modes. These displays can be visualized as far-field directivity patterns. The pattern for each mode is seen to consist of a principle lobe that dominates over a variable number of side lobes. The mode levels as shown with $A_{m,\mu}$ constant are defined as equal amplitude modes.

The approximate angular location of the peak of the principle lobe $(\phi_1)_p$, is simply given by

$$(\phi_1)_p = \sin^{-1} \frac{k'_{m,\mu}}{\bar{k}} \qquad (4)$$

with no flow, $k'_{m,\mu}/\bar{k}$ is reduced to $1/\xi$ (Eq. (2) with $M = 0$) and thus

$$(\phi_1)_p = \sin^{-1} \frac{1}{\xi} \qquad (5)$$

As seen in Fig. 10 the peak for some principle lobes actually occurs at a value of $\bar{k} \sin \phi_1$ larger than, $k'_{m,\mu}$ and, therefore, at a larger angle than that given by Eq. (4). The determination of the exact peak location was discussed by Saule in Ref. 9.

The angular location of the principle lobe peak is a property often used to identify a mode in far-field directivity patterns. As a point of reference for subsequent adjustments, the location of the peak with no flow $(\phi_1)_p$, for the (0,1) and (13,0) modes varies with engine speed as shown in Fig. 11. The plane wave (0,0) mode is not shown because it peaks on axis at all speeds and requires no adjustments.

Flow Everywhere. Candel[5] has shown that the radiation patterns with flow in the far-field equal to that in the duct can be related to the radiation obtained without flow by a coordinate stretching technique. As a result of his analysis the directivity angle with the same flow everywhere, ϕ_2, is related to the angle without flow, ϕ_1, and the flow Mach number, M, by

$$\phi_2 = \tan^{-1} \frac{\sin \phi_1}{f_1} \qquad (6)$$

where $f_1 = [1 - \sin^2\phi_1(1 - M^2)]^{1/2}$

As given in Ref. 7, this transformation of variables locates the principle lobe peak as a function of cutoff ratio, ξ, as follows.

$$(\phi_2)_p = \cos^{-1}\left\{\frac{(1 - M^2)[1 - (1/\xi^2)]}{1 - M^2[1 - (1/\xi^2)]}\right\}^{1/2} \qquad (7)$$

The angular locations of the principle lobe peak $(\phi_2)_p$, are also shown for the (0,1) and (13,0) modes in Fig. 11. Flow everywhere is seen to cause relatively small angular displacements toward the axis.

Duct Flow Alone. As discussed by Rice, et al.[7] the radiation directivity with flow everywhere includes a convective effect due to the flow in the far-field. The directivity angles with far-field convection, ϕ_2, and without the convection, ϕ_3, are related to each other by

$$\tan \phi_2 = \frac{\tan \phi_3}{1 - M/\cos \phi_3} \qquad (8)$$

Using this relation, the directivity angle ϕ_3 can be related to the no flow angle ϕ_1, by

$$\phi_3 = \cos^{-1} \frac{M + f_1}{1 + Mf_1} \qquad (9)$$

where f_1 is the directivity transformation function used in Eq. (6). The approximate angular location of the principle lobe peak[7] is related to the mode cutoff ratio, ξ, by

$$(\phi_3)_p = \cos^{-1} \frac{M + \sqrt{1 - 1/\xi^2}}{1 + M\sqrt{1 - 1/\xi^2}} \qquad (10)$$

For convenience, a flow direction into the inlet was designated as positive in expressing Eqs. (8) to (10). The opposite designation is often used.[5-7]

The variations of $(\phi_3)_p$ are also shown in Fig. 11. With duct flow alone the principle lobe peak beams significantly closer to the inlet axis than for the case of flow everywhere.

In Ref. 7 modes were characterized by direction angles within the duct. The angle $(\phi_3)_p$ is identical to the direction angle of the mode with respect to the duct axis. It was postulated in Ref. 7 that the mode would beam from the duct and into the far-field at this angle.

Refraction Effects. The effects of transmitting radiation from within a duct with flow to a region of no flow outside the duct have been neglected in defining the duct flow alone angle, ϕ_3.

Potential flow solutions provide explicit flow variations in this transitional region that may be useful in calculating its effect on directivity. The effect can also be approximated as a refraction process at an interface, as suggested in Ref. 10, with the interface being similar to a potential contour relatively close to the inlet.

Such a refractive process is illustrated in Fig. 12. The refracted angle, ϕ_r, is larger than the incident angle, ϕ_i, because the acoustic wave travels at less than the speed of sound in approaching the interface. Refraction, however, can have opposite effect on directivity angles as shown in Fig. 12. For the interface shown refraction is toward the axis when the radiation angle is greater than 45° and toward the sideline when smaller. It is interesting to note that an interface normal to the inlet axis gives a calculated refraction that is nearly identical to the far-field convective effect. No attempt will be made to quantify the refractive process in this study but its qualitative effects on directivity will be recognized in comparing predicted and measured radiation patterns.

Modal Phase. The radiation patterns resulting from two or more simultaneously propagating modes require that far-field pressures be summed as complex variables. In performing the summation, the principle and side lobes of a particular mode can be considered regions of reinforcement and rarefaction as described for radial pressure profiles within the duct (Fig. 9). Adjacent far-field lobes of a single mode are 180 degrees out-of-phase. The relative phase between the modes, however, must be established to perform a summation.

Although two modes may be generated at a particular relative phase, a continuous shift of relative phase occurs as they propagate through a duct. The phase shift is caused by the difference between their axial wave number or axial phase velocities. The calculated phase shift between the (0,0) and (0,1) modes after propagating through the 0.55 m (21.75 in.) cylindrical section of the engine inlet varies with engine speed as shown in Fig. 13(a). The phase shift is significant but relatively small for these two highly propagating modes. The phase shift becomes negligible for modes with $\xi >> 1$.

A change in inlet length will also alter the relative phase between two modes. Tests made with a 0.1 m (4 in.) length change for the 41 rod array were made for this purpose. The calculated shift in relative phase caused by this length change varies with speed as shown in Fig. 13(b). The phase shift shown can significantly alter far-field radiation patterns. This is illustrated in Fig. 14 where summations of the (13,0) and (13,1) modes for several relative phases are shown. The region between the two principle lobes is seen to be most sensitive to changes in relative phase. The effect would be less evident if the modes differed significantly in amplitude. The tests with a 0.1 m (4 in.) change in inlet length were an attempt to test these concepts.

It should be noted that whereas combined patterns are axisymmetric for modes of the same m order they are generally asymmetric for modes of differing m order.

Results and Discussion

A more detailed analysis and discussion of the tone noise generated by the rods will be presented based on the concepts of the previous section. In order to more clearly isolate the tone noise generated by the rods, the data to be used are sound pressure levels of the differences in one-third-octave band pressures of the BPF tone measured with and without rods. Small differences giving erratic results will be neglected.

28-Rod Array

The 28 rod array was predicted to generate the plane wave (0,0) mode and at least one other axisymmetric mode. Measurements made with pole microphones clustered near the inlet axis are best used to identify such modal properties. Figure 15 shows the data and predicted principle lobes for the (0,0) and (0,1) modes at levels adjusted to fit the data. The (0,0) mode alone has a lobe centering on the axis whereas all other modes do not radiate on the axis. The comparisons shown in the figure indicate that the (0,0) mode is present at all speeds and dominant except at 10,500 rpm. Presence of the (0,1) mode is also implied but at a lower level except at 10,500 rpm. Why this 10,500 rpm condition is an exception is not known. In general, the (0,0) and (0,1) modes differ in level by roughly 15 dB. The result implies equal amplitude modes ($A_{m,\mu}$ constant) where, as displayed in Fig. 10(a), the (0,1) mode peak is about 16 dB below the (0,0) mode peak when amplitudes are equal.

The (0,0) and (0,1) modes were expected to be generated at a relative phase of 180° and propagate to the far-field following some phase shift within the inlet duct. Figure 16 compares the data at 6750 and 8450 rpm with predicted patterns that accounts for the expected relative phase of the (0,0) and (0,1) modes. The expected relative phase at these two speeds after traversing the duct is about the 135° shown. (Figure 13(a) indicate a phase shift within the duct of about 45° in this region of engine speed.) As will be shown later, directivity angles can not be too closely scrutinized in such comparisons because of refraction at the inlet face. Figure 16, however, implies that the initial generation of these modes with a relative phase of 180° is probable.

Directivity patterns obtained with the ground based microphones are compared with predictions in Fig. 17. (The previous pole microphone data are

not combined with this data because of uncertain ground reflections.) The angular spacing of the microphones for the data in Fig. 17 is too large to reveal detailed modal structure. The predicted curves, therefore, are simply envelopes of the principle lobe peaks of the possible modes at equal amplitudes ($A_{m,\mu}$ constant). Envelopes assuming duct flow alone, ϕ_3, as well as flow everywhere, ϕ_2, are shown. Both envelopes are shown because, as described later they essentially bracket the expected radiation pattern with refraction at the inlet.

In general, the data in Fig. 17 imply that the decrease in modal level with increasing radial order is larger than that for equal amplitude modes. The exceptions involving individual data points imply an absence of a particular mode. For example, at 6750 rpm the (0,3) mode and at 8450 rpm the (0,4) mode appear to be absent. The absence of modes depends on details of the tone generation process. The sparcity of this data does not permit a detailed evaluation of modal structure. These data, however, do not refute those from the pole microphones where the (0,0) and (0,1) modes were identified.

41 Rod Array

Measured and predicted directivities for the 41 rod array are compared in Fig. 18. The predictions consist of the principle lobe of the (13,0) mode assuming both duct flow alone and flow everywhere. A particular discrepancy between theory and data to be noted first is evident at the 6750 rpm speed. The measured pattern is seen to be lobular whereas the predicted patterns are not. This difference is at least in part the consequence of using the flanged duct radiation function for a near cutoff mode as generated at the 6750 rpm speed. For a flangless duct the predicted levels would continuously decrease toward and past 90° and the pattern would be lobular. This limitation of the flanged duct predictions, however, does not apply to the principle lobes of the more highly propagating modes at the other speeds in Fig. 18.

Observing for the moment only the angular bandwidth of the predicted lobes, a dominant feature appears to be that the data correspond to the principle lobe for a single mode. Although more than one mode can propagate above 8450 rpm the data imply relatively low amplitudes for the higher radial orders of the m equal 13 modes. The (13,0) mode appears dominant as qualitatively expected from excitation by rods located near the outer wall.

With regard to the two predictions the data do not consistently agree with either prediction. The prediction for duct flow alone was expected to apply if refraction at the inlet face was negligible or small. Agreement exists at 8450 rpm but at higher speeds this prediction is biased more toward the inlet axis than the data. The flow everywhere prediction is as good or better at the higher speeds.

Refraction at the inlet face can be used to explain the deviations between predicted and measured patterns shown in Fig. 18. It was noted in Fig. 12 that refraction should be toward the sideline for small radiation angles and comparable to that obtained from flow everywhere. At larger radiation angles no refraction or refraction toward the axis may be expected. Inspection of the predicted (ϕ_3) and measured patterns reveals that refraction at an interface comparable to that illustrated in Fig. 12 would qualitatively explain the observed principle lobe peak directivities. At 45° (8450 rpm) there is no refraction because the lobe peak beams normal to the interface. At smaller angles (higher speeds) the peak is refracted toward the sideline and at larger angles (6750 rpm) refraction is toward the axis. It appears that ϕ_3 does characterize modal radiation upon leaving the duct (no refraction) as postulated in Ref. 7.

Although refraction is implied it has not been proven and requires additional study. Refraction, however, would impact the prediction of flight noise from ground static test data. The velocity gradient at the inlet face that can cause refraction become less severe during forward motion and essentially disappear at some flight speed. The static test data, therefore, would require adjustments for changes in refraction when applied to flight calculations. Figure 18 indicates angular adjustments as large as 10° may be needed for radiation at intermediate angles from the inlet axis.

The measured patterns beyond the principle lobe can not be exactly diagnosed because of both the variety in possible modal combinations and the limitations of the flanged duct radiation theory. Figure 19, however, schematically illustrates combinations of approximate modal directivity patterns that may simulate this region for the 9,600 and 10,500 rpm tests. It appears that the level of the (13,1) mode is at least 10 dB lower than the (13,0) mode. The data should agree with the summation of these modes. The summation, however, is dependent on relative phase. The region most sensitive to relative phase is at the intersection of principle lobes where either complete cancellation or reinforcement can occur. Sensitivity of this region to modal phase will be evident in the subsequent results obtained with an inlet length change.

Inlet Length Change

Tone directivities obtained with inlet lengths differing by 4 inches are compared in Fig. 20. The length change was predicted to change the relative phase between two modes and thus their directivity patterns. No effect was expected at 6750 and 8450 rpm because only a single mode propagates. The data at these speeds are similar although there are small differences for unknown reasons. The presence of some lower circumferential order modes caused by imperfect rotor blade or rod spacing could give the observed change. An expected change in directivity as described in discussing Fig. 19 is exhibited at 9,600 and 10,500 rpm. Changes are strongly evident near the intersection of (13,0) and (13,1) mode principle lobes. Variable summing of side lobes is the probable cause of the variations evident at the higher inlet angles. These results at 9,600 and 10,500 rpm appear to confirm that relative modal phase is altered by an inlet length change.

The results at 13,500 rpm in Fig. 20 are not simply explained. Tone noise generated by the rods at this speed was evident at inlet angles as low as 6°. This infers that highly propagating modes,

other than the m=13 family, are present. With additional modes such directivity changes are possible.

Rotor Alone Tone

A final observation regarding modal directivities concerns the rotor alone tone. At 13,500 rpm this tone should simply propagate as the (28,0) mode at a cutoff ratio of 1.08. This mode is clearly evident in the directivity patterns both with and without rods in Fig. 5(b). The principle lobe of the (28,0) mode is the lobular pattern peaking at about 60°. It is instructive to compare the directivity of this mode with that of the (13,0) mode generated by the 41 rods at 6750 rpm. The cutoff ratio of the (13,0) mode at this speed is 1.05. The calculated directivity patterns for the two modes are nearly identical. The measured patterns are compared in Fig. 21 and near identity of the patterns extends to an inlet angle of 120°. This pattern, therefore, appears to characterize the radiation of a near cutoff mode from the bellmouth inlet used on the JT15D engine. This pattern differs significantly from that calculated for a flanged duct (Fig. 18) as was discussed earlier.

Concluding Remarks

These experiments with inlet rods in the JT15D engine demonstrate the general validity of modal generation, propagation and radiation theory under actual engine operating conditions. The data provided one of few opportunities to analyze dominant modes propagating under relatively high duct flow conditions. As postulated in Ref. 7, with duct flow alone (as in static engine tests) the directivity angle of the beamed radiation of a mode, upon leaving the duct, appears to agree with the axial propagation angle characterizing the mode within the duct. A qualitative accounting for of refraction effects at the inlet face was used, however, to obtain the agreement. The refraction effects require a more thorough study in conjunction with more precise solutions for modal radiation from an engine inlet. Refraction, if as significant as indicated, could impact static/flight noise comparisons and predictions.

References

1. Jones, W. L., McArdle, J. G., and Homyak, L., "Evaluation of Two Inflow Control Devices for Flight Simulation of Fan Noise Using a JT15D Engine," AIAA Paper 79-0654, Mar. 1979.

2. Tyler, J. M. and Sofrin, T. G., "Axial Flow Compressor Noise Studies," SAE Transactions, Vol. 70, 1962, pp. 309-332.

3. Kobayashi, H. and Groeneweg, J. F., "Effects of Inflow Distortion Profiles on Fan Noise Calculated Using a 3-D Theory," AIAA Paper 79-0577, Mar. 1979.

4. Saule, A. V., "Modal Structure Inferred from Static Far-Field Noise Directivity," AIAA Paper 76-574, July 1976, also NASA TM X-71909, 1976.

5. Candel, S. M., "Acoustic Radiation from the End of a Two-Dimensional Duct - Effects of Uniform Flow and Duct Lining," Journal of Sound and Vibration, Vol. 28, May 1973, pp. 1-13.

6. Homicz, G. F. and Lordi, J. A., "A Note on the Radiative Directivity Patterns of Duct Acoustic Modes," Journal of Sound and Vibration, Vol. 41, Aug. 1975, pp. 283-290.

7. Rice, E. J., Heidmann, M. F., and Sofrin, T. G., "Modal Propagation Angles in a Cylindrical Duct with Flow and Their Relation to Sound Radiation," AIAA Paper 79-0183, Jan. 1979, also NASA TM-79030, 1979.

8. Lansing, D. L., Drischler, J. A., and Pusey, C. G., "Radiation of Sound From an Unflanged Circular Duct with Flow," paper presented at the 79th Meeting of the Acoustical Society of America, Atlantic City, April 21-24, 1970.

9. Saule, A. V. and Rice, E. J., "Far-Field Multimodal Acoustic Radiation Directivity," paper presented at the 94th Meeting of the Acoustical Society of America, Miami Beach, Florida, December 12-16, 1977; also NASA TM-73839, 1977.

10. Benzakein, M. J., Claes, H. P., Coward, W. E., Hochheiser, R. M., Kazin, S. B., "Fan/Compressor Noise Research, Volume I: Detailed Discussion," FAA-RD-71-85-Vol. 1, Oct. 1971. (AD-740513)

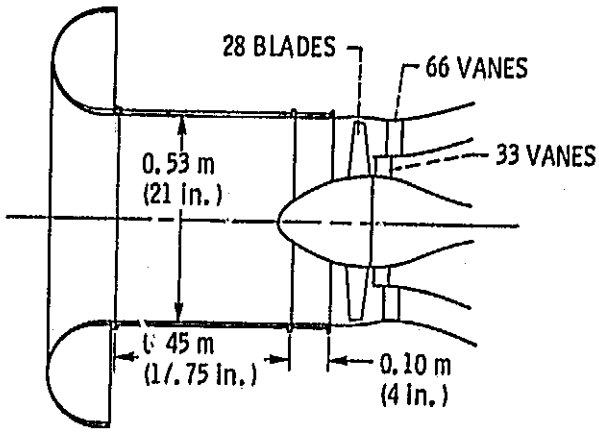

Figure 1. - JT15D inlet configuration.

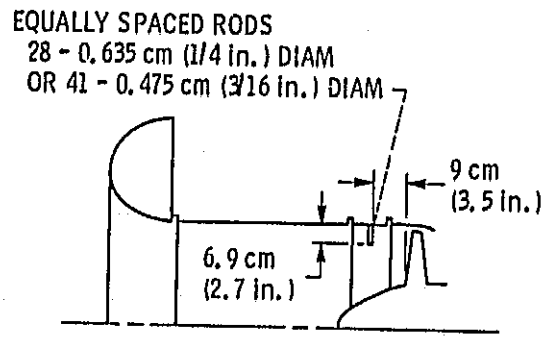

Figure 2. - Rod installation.

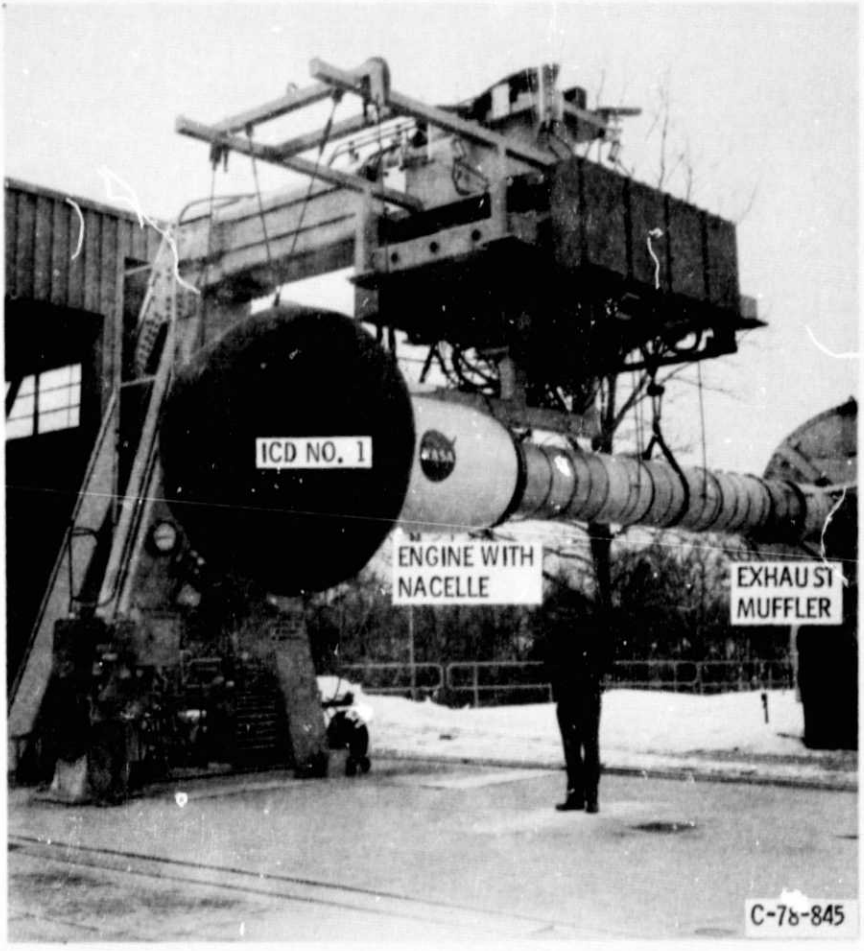

Figure 3. - JT15D engine with ICD on VLF Facility.

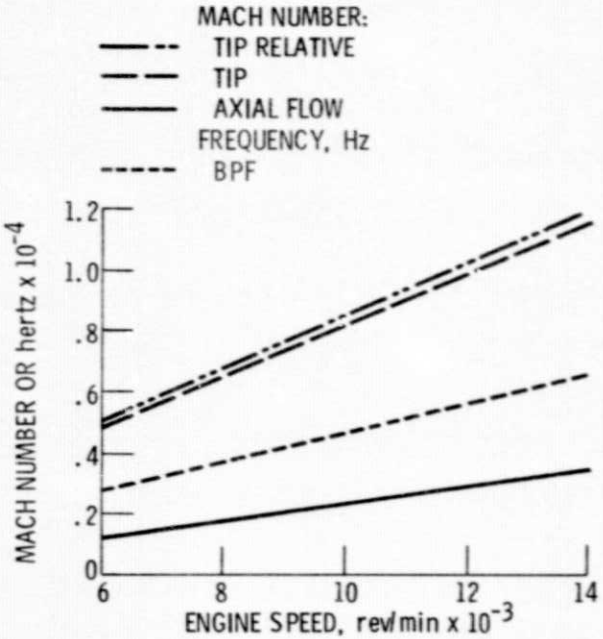

Figure 4. - Engine performance properties.

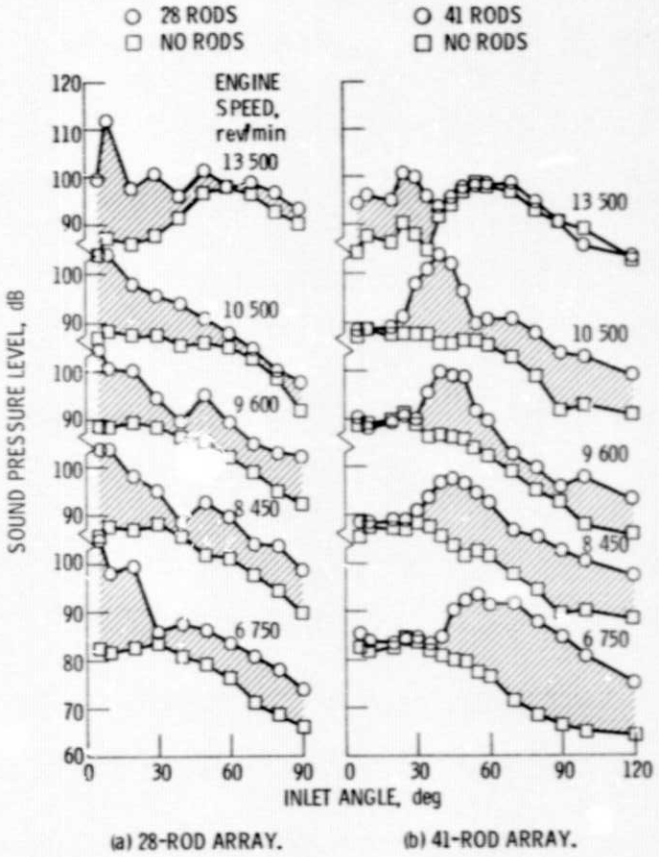

(a) 28-ROD ARRAY. (b) 41-ROD ARRAY.

Figure 5. - Effect of rods on 1/3-octave band BPF tone directivities.

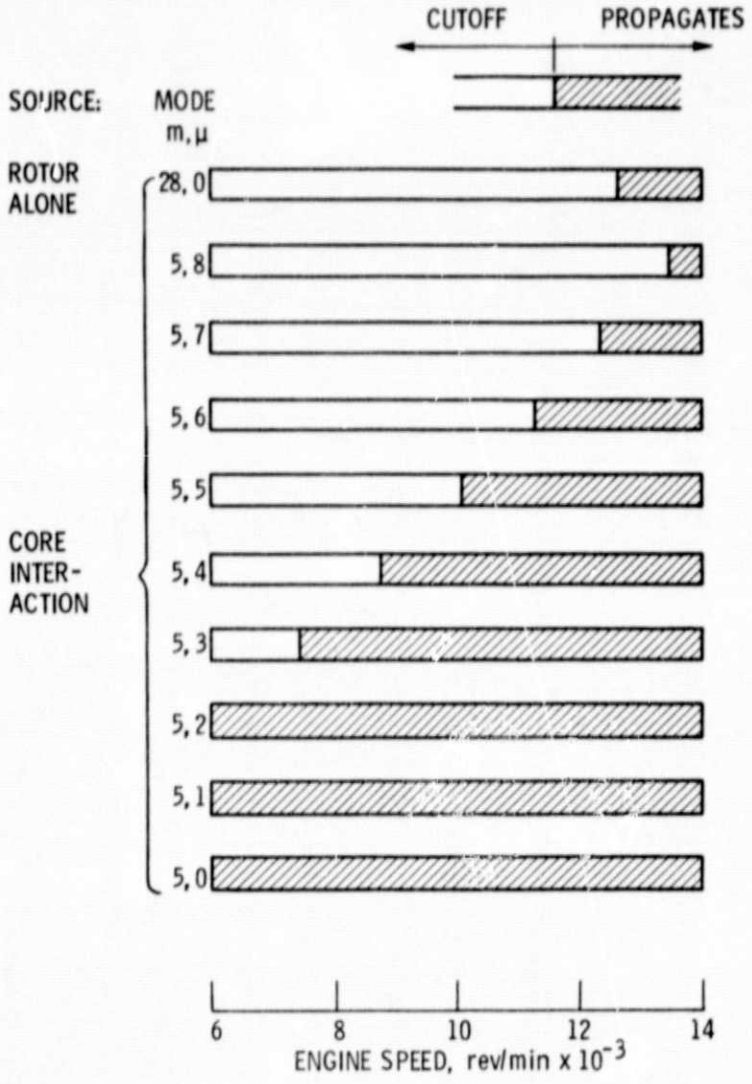

Figure 6. - Propagating BPF modes of engine without rods.

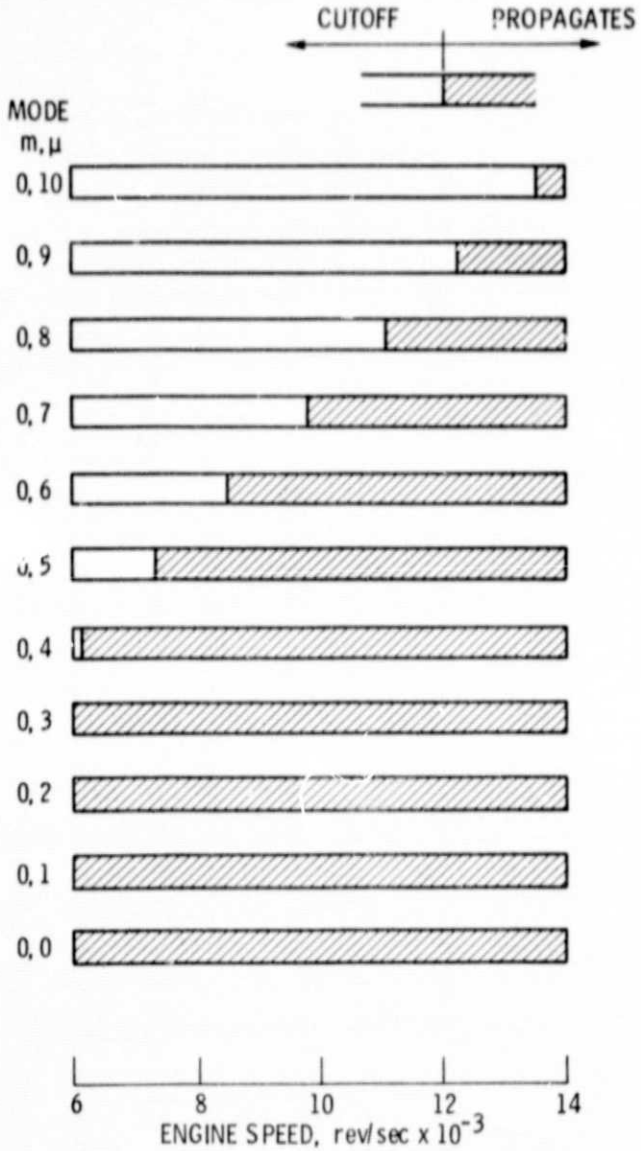

Figure 7. - Propagating BPF modes for interaction of 28 rods with rotor.

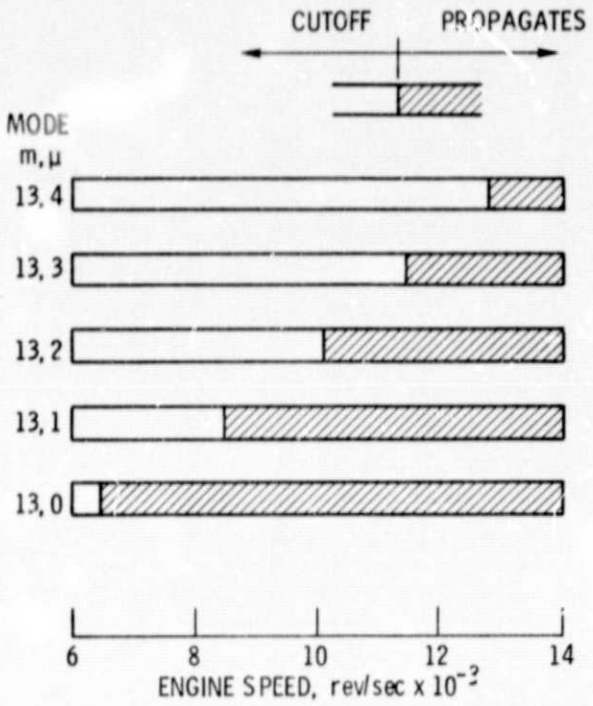

Figure 8. - Propagating BPF modes for interaction of 41 rods with rotor.

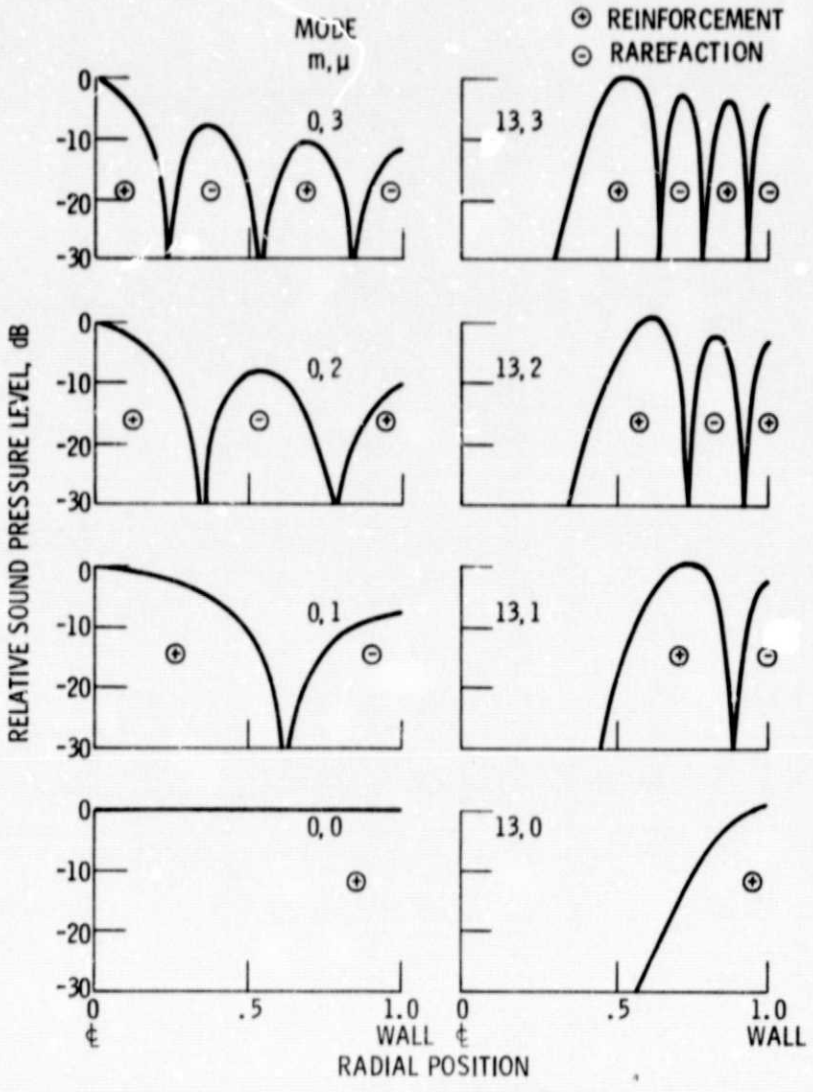

(a) INDIVIDUAL MODES.

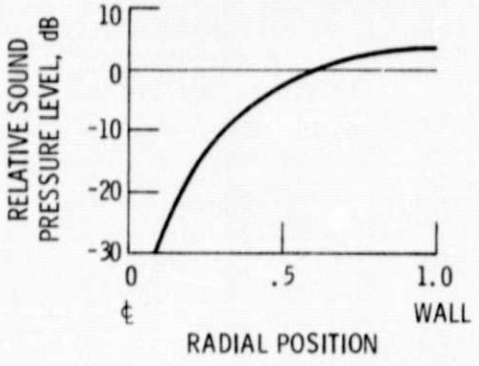

(b) INVERSE SUMMATION OF (0, 0) AND (0, 1) MODES.

Figure 9. - Radial profiles of sound pressure levels of modes within the duct.

E-9691

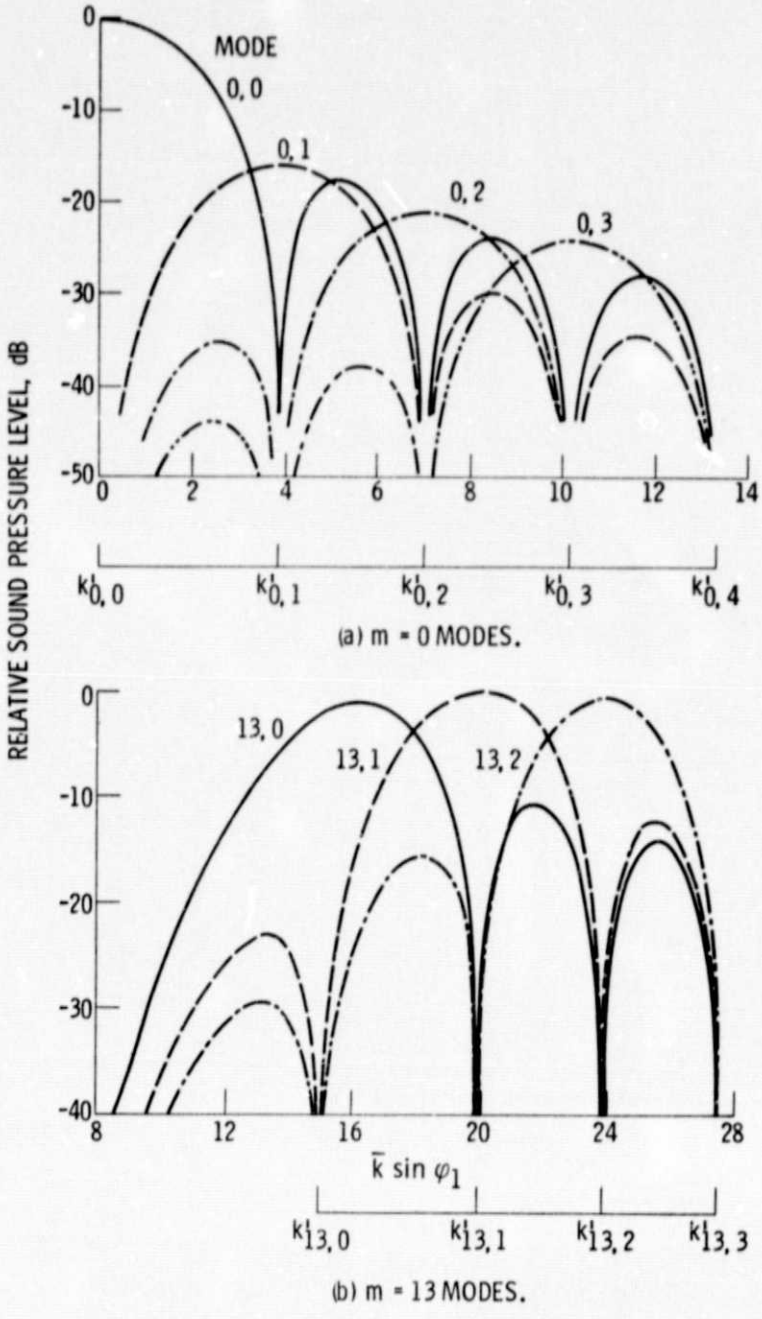

Figure 10. - Display of far-field directivity function (eq. (3)).

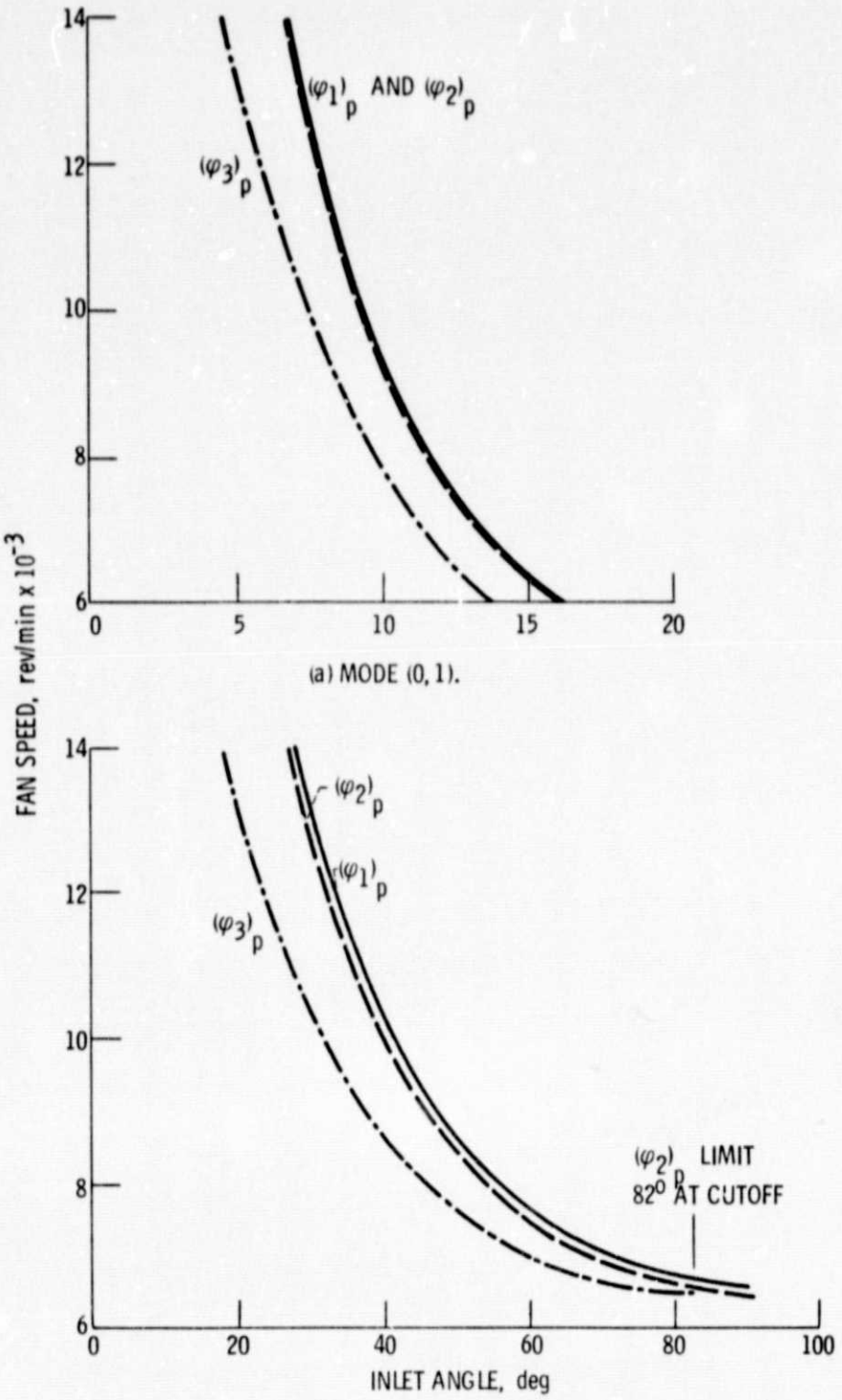

Figure 11. - Directivity angles of principle lobe peak.

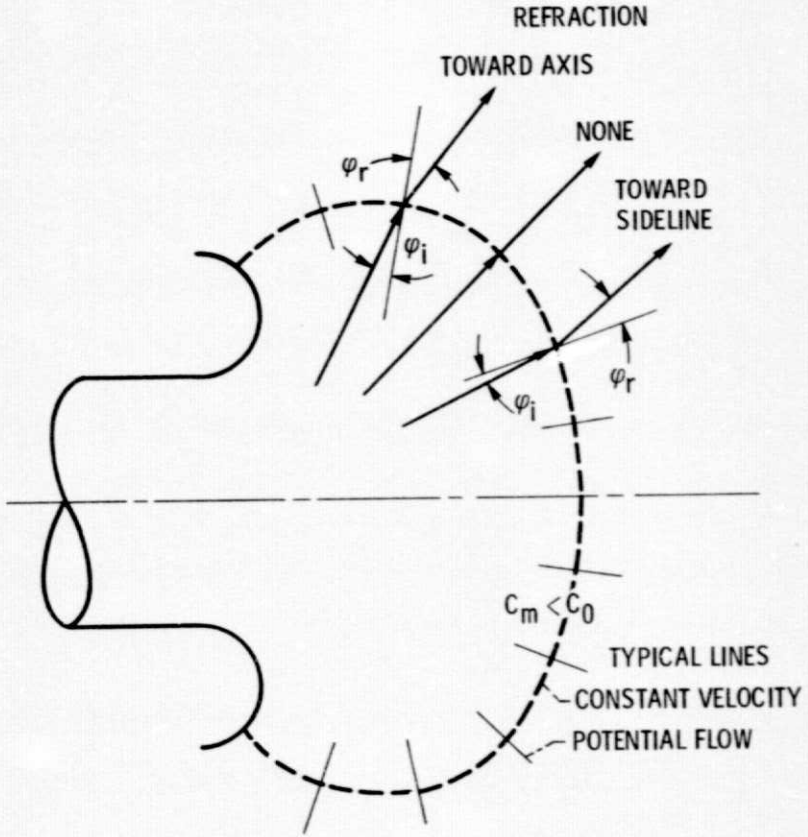

Figure 12. - Refraction from velocity gradients near inlet face.

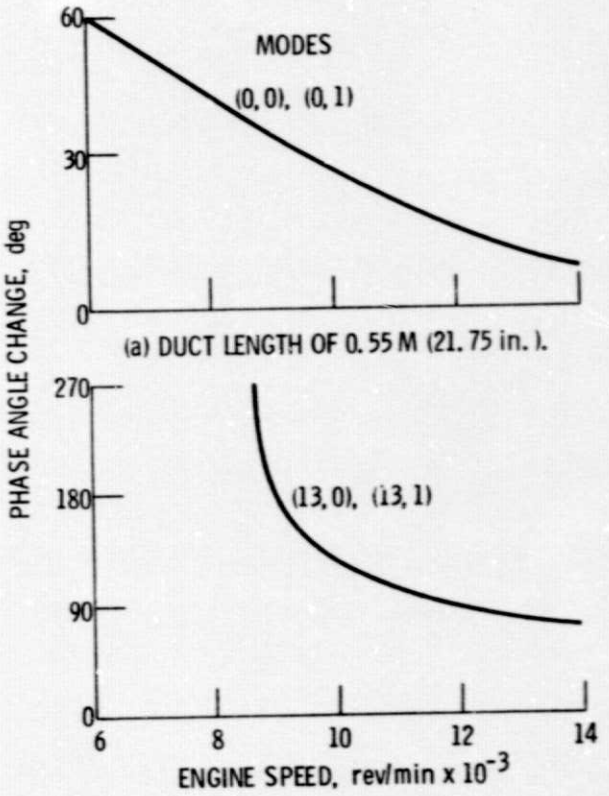

(a) DUCT LENGTH OF 0.55 M (21.75 in.).

(b) DUCT LENGTH CHANGE OF 0.1 M (4 in.).

Figure 13. - Effect of duct propagation on relative phase between modes.

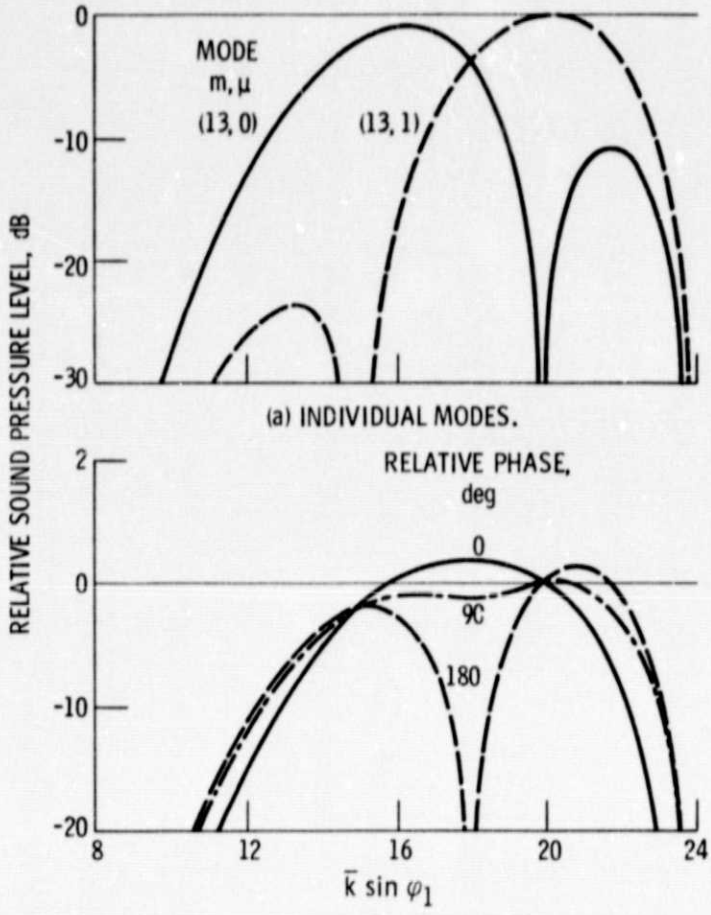

Figure 14. - Effect of modal phase on summation of modes.

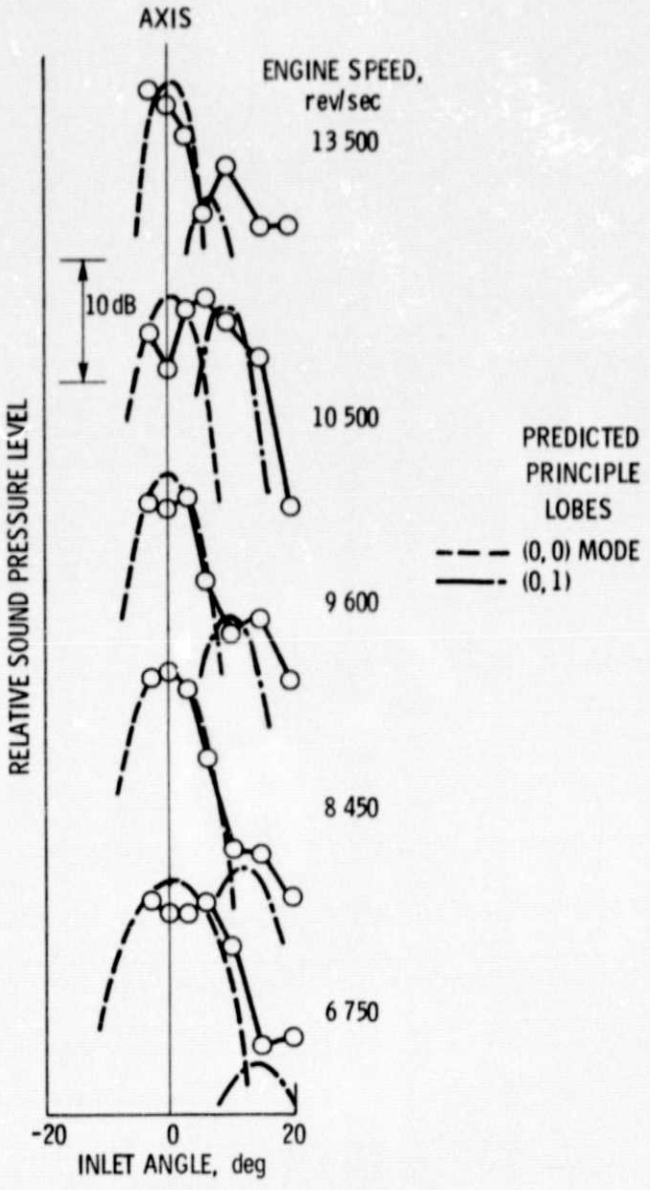

Figure 15. - Directivity patterns for 28 rod array from pole microphones near inlet axis.

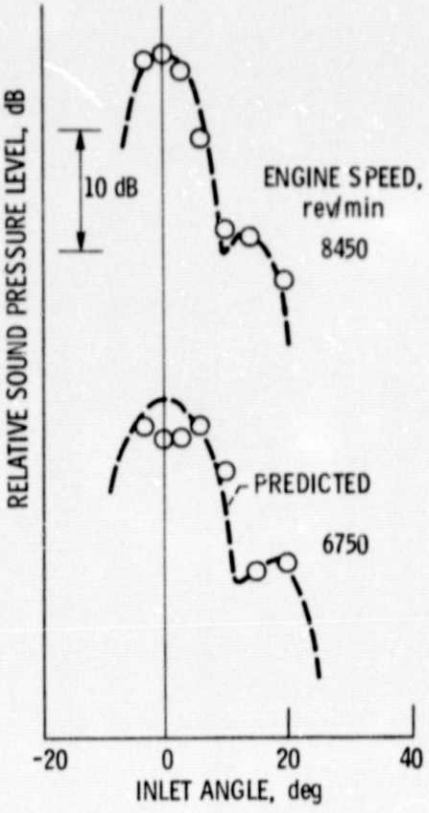

Figure 16. - Comparison of pole microphone data with combined (0, 0) and (0, 1) pattern at a relative phase of 135 deg.

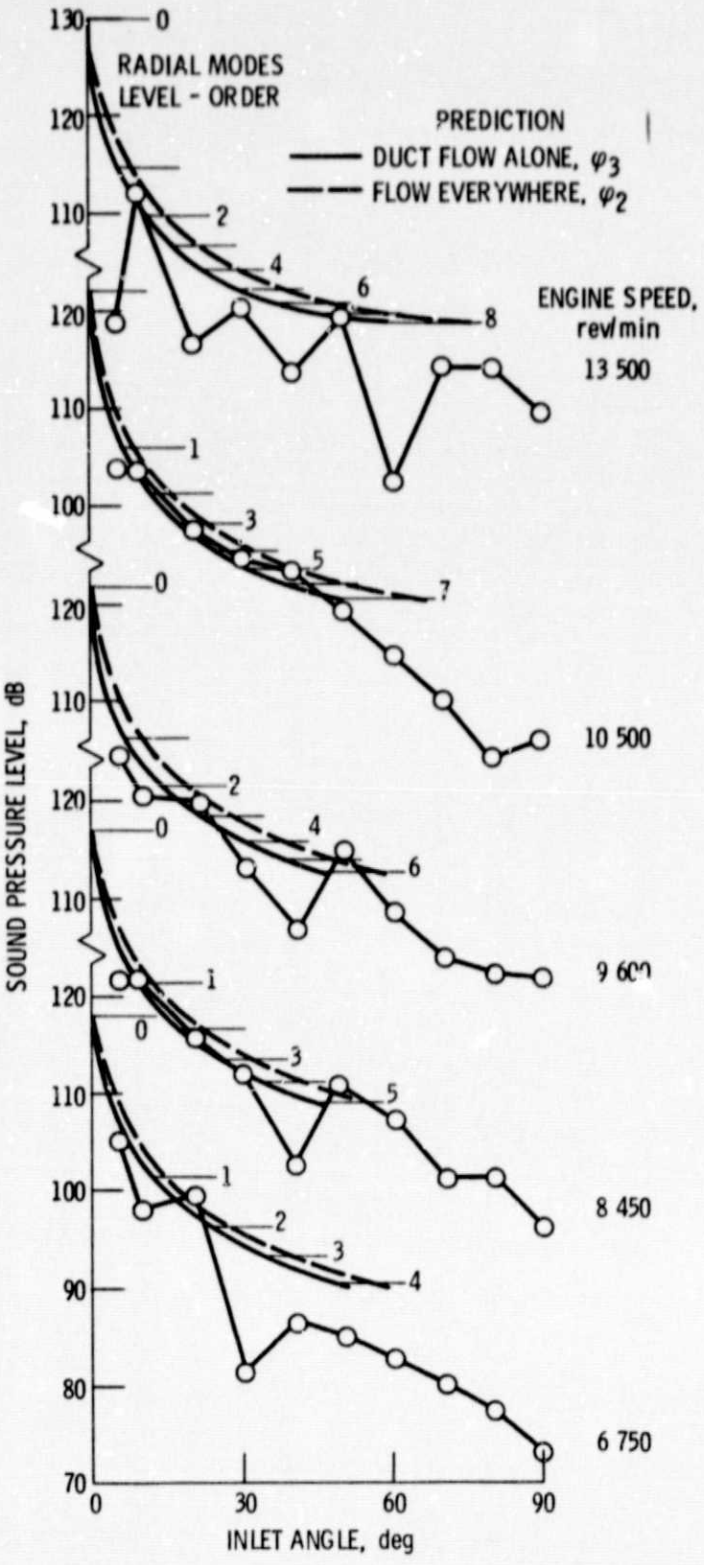

Figure 17. - Comparisons of predicted envelopes of equal amplitude m = 0 modal peaks with 28-pod array BPF tone directivities.

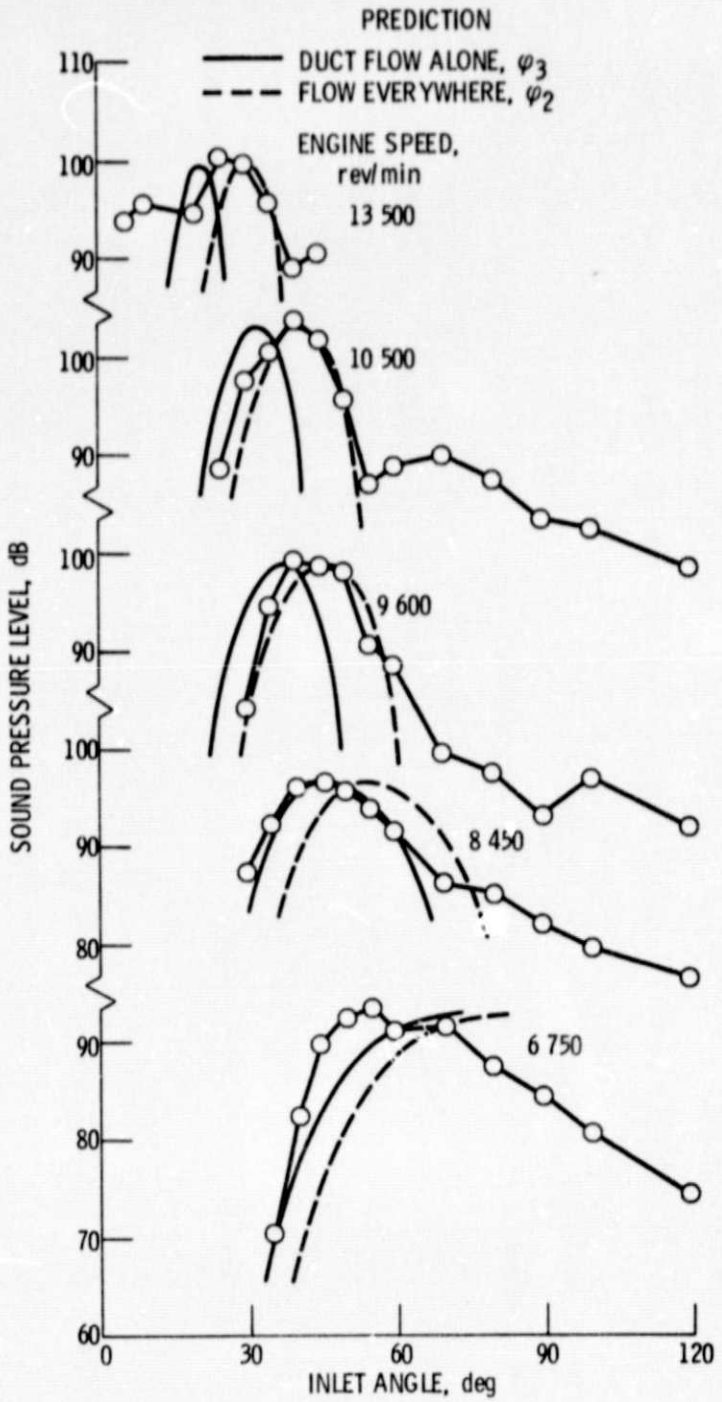

Figure 18. - Comparison of measured and predicted BPF tone directivities for 41-rod array.

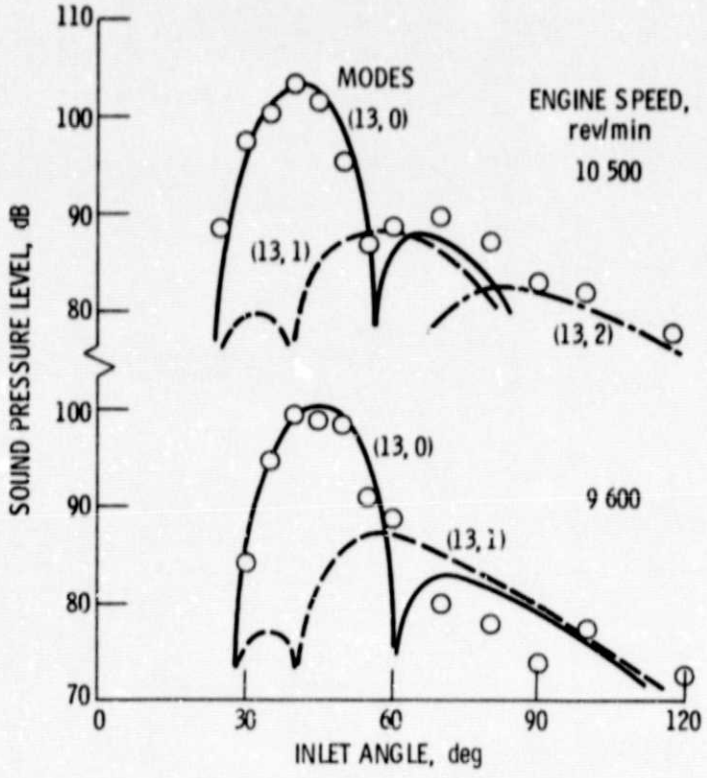

Figure 19. - Characterization of 41-rod array data with approximations of modal radiation properties.

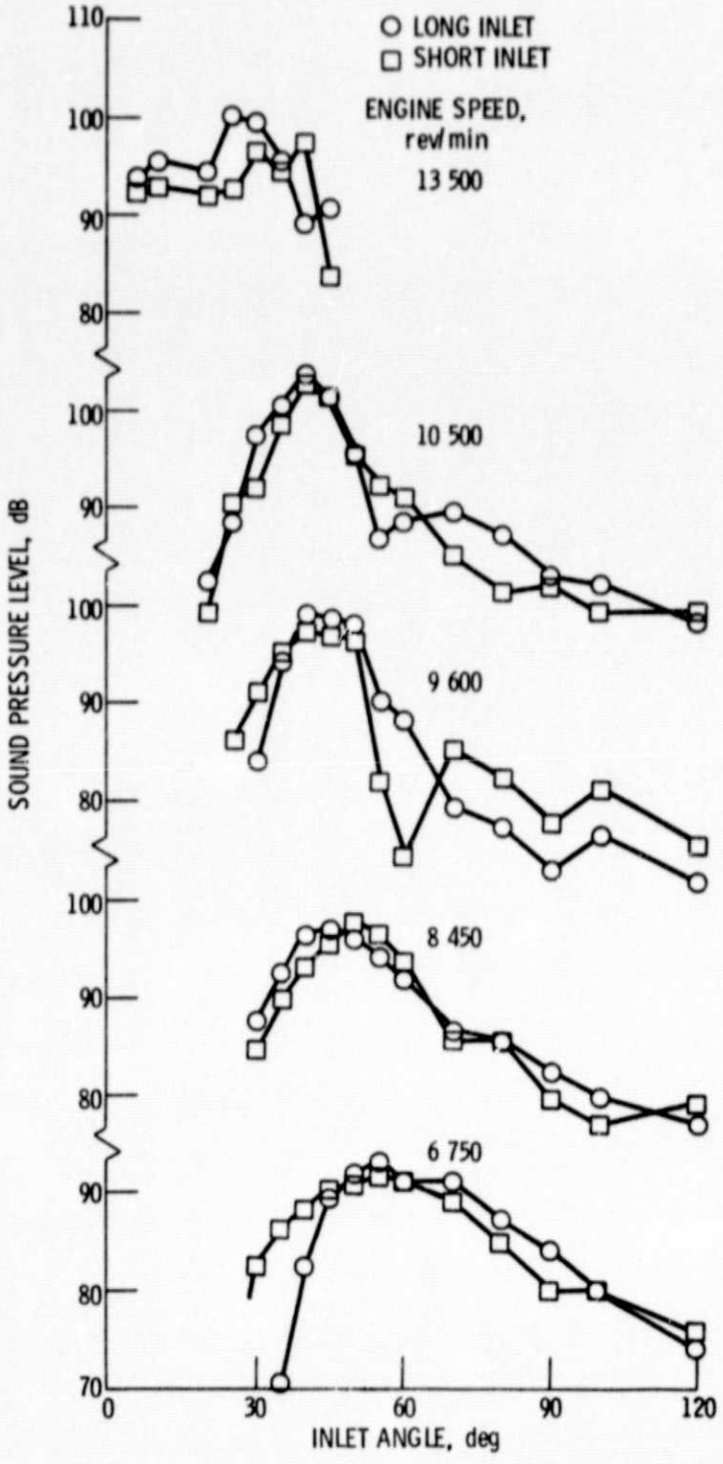

Figure 20. - Experimental effect of 4 inch inlet length change of BPF tone directivities for 41-rod array.

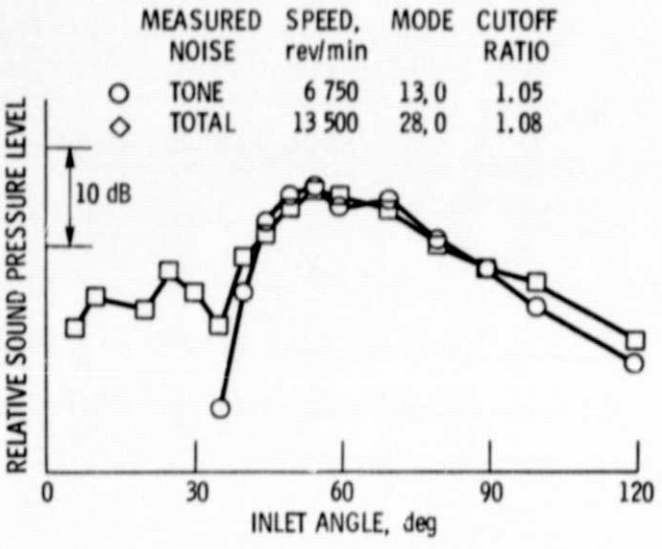

Figure 21. - Directivity comparison of rotor alone tone and 41-rod array tone at near-cutoff conditions.